

TOWARDS 20 % EFFICIENT N-TYPE SILICON SOLAR CELLS WITH SCREEN-PRINTED ALUMINIUM-ALLOYED REAR EMITTER

Christian Schmiga, Martin Hermle and Stefan W. Glunz
Fraunhofer Institute for Solar Energy Systems (ISE)
Heidenhofstraße 2, 79110 Freiburg, Germany

Phone: +49(0)761/4588-5201, Fax: +49(0)761/4588-9250, E-mail: christian.schmiga@ise.fraunhofer.de

ABSTRACT: We present *n*-type silicon solar cells featuring an effectively passivated full-area screen-printed aluminium-alloyed rear emitter. Two different passivation stacks for Al-*p*⁺ emitters are investigated: The first one consists of a plasma-enhanced-chemical-vapour-deposited amorphous silicon film covered by a plasma silicon oxide layer, the second one of a plasma-assisted atomic-layer-deposited aluminium oxide also covered by a plasma silicon oxide. For our a-Si/SiO_x-passivated back junction *n*⁺*np*⁺ solar cells (4 cm²) we achieve an increase in the open-circuit voltage of 15–20 mV compared to the non-passivated emitter cells, for our Al₂O₃/SiO_x-passivated cells the shift amounts to 25–30 mV, resulting in *V*_{oc} values up to 655 mV. This leads to record-high efficiencies for solar cells with aluminium-doped emitter of 19.5 % and 20.1 %, respectively, on *n*-type phosphorus-doped 10 Ωcm float-zone silicon material.

Keywords: *n*-type Solar Cells, Aluminium-alloyed emitter, Passivation

1 INTRODUCTION

n-type silicon (*n*-Si) has been proven to be a high-quality silicon material due to its larger tolerance to most common impurities (e. g. Fe) compared to *p*-type Si, resulting in higher minority carrier diffusion lengths [1]. Additionally, *n*-Si is free of light-induced degradation related to boron-oxygen complexes. However, recently it has been reported that *n*-type multicrystalline (mc) Si appears to be less attractive for the application to rear junction cells than previously assumed [2, 3]. From this, it can be concluded that (i) the production of *n*-type rear junction cells has to be restricted to monocrystalline (mono) Si because of its lower impurity concentration or that (ii) an adequate processing technology for front junction *n*-type mc Si cells has to be developed.

In this paper, we focus on *n*-type solar cells fabricated on mono Si substrates. The two only companies, SunPower and Sanyo, which produce high-efficiency solar cells today are using *n*-type mono Si wafers which further supports the large potential of this material for the application to industrial high-efficiency cells. In the following, a short review of monocrystalline *n*-type silicon solar cells is given separated by the three different techniques for the *p*⁺ emitter formation:

1.1 Boron-diffused Emitters

Recently, Benick *et al.* [4] have achieved an efficiency of 23.2 % for a front junction passivated emitter with rear locally diffused (PERL) solar cell (4 cm²) on 1 Ωcm *n*-type float-zone (FZ) Si. Mihailtchi *et al.* [5] reported an efficiency of 18.3 % for a large-area (156 cm²) screen-printed Cz Si (1.5 Ωcm) solar cell. *n*-type cells (146 cm²) with front boron emitter have also been fabricated by Buck *et al.* [6], reaching efficiencies of 17.1 % on 2 Ωcm Cz Si.

For passivated emitter with rear totally-diffused solar cells (22 cm²) featuring a boron-doped rear emitter (re-PERT), Zhao *et al.* [7, 8] demonstrated efficiencies of 22.7 % on 1.5 Ωcm FZ Si substrates and 20.8 % on 5 Ωcm Czochralski-grown (Cz) Si wafers. Guo *et al.* [9] presented laser-grooved interdigitated backside buried

contact (IBBC) cells (8 cm²) with efficiencies of 19.2 % on 1 Ωcm FZ Si and 16.8 % on Cz Si. Froitzheim *et al.* have obtained efficiencies up to 17.4 % for large-area (149 cm²) screen-printed *n*-type Cz Si cells with a boron-diffused back junction [10]. Conversion efficiencies of 22.7 % have been reported by De Ceuster *et al.* [11] for SunPower's back-contact solar cell on *n*-type FZ Si material. Cells (149 and 155 cm²) with an efficiency mode of 22.4 % are manufactured in the latest production line.

1.2 Amorphous Si/Crystalline Si Heterojunctions

Sanyo's heterojunction with intrinsic thin layer (HIT) solar cell reaches efficiencies of 22.3 % on *n*-type Cz Si wafers (100.5 cm²) which has been published by Taira *et al.* [12]. In mass production, an averaged cell efficiency of 19.5 % is obtained [13]. Conrad *et al.* [14] have fabricated 19.8 % efficient a-Si/c-Si cells without additional intrinsic buffer layer on *n*-type Si substrates.

1.3 Aluminium-alloyed Emitters

For *n*⁺*np*⁺ solar cells (4 cm²) featuring an aluminium-doped emitter on the rear side formed by annealing of evaporated high-purity aluminium, Cuevas *et al.* [15] have achieved efficiencies up to 16.9 % on 80 Ωcm FZ Si material. Using laser-fired local Al emitters (LFE), Glunz *et al.* [16] have obtained 19.4 % on 100 Ωcm FZ Si (4 cm²). By applying a full-area screen-printed Al-*p*⁺ emitter, Schmiga *et al.* [17] demonstrated efficiencies of 18.9 % on 4 Ωcm Cz Si (4 cm²).

For front and rear screen-printed *n*-type cells with Al-*p*⁺ back junction, several results have been published during recent years: Hacke *et al.* [18] reported an efficiency of 15.0 % for the PhosTop cell (100 cm²) on 1 Ωcm FZ Si. Buck *et al.* [19] and Kopecek *et al.* [20] attained efficiencies of 15.3 % on 5 Ωcm Cz Si (4 cm²) and 16.4 % on 20 Ωcm FZ Si (150 cm²), respectively. Schmiga *et al.* [21] and Nagel *et al.* [22] achieved an efficiency of 17.0 % on 4 Ωcm Cz Si material (100 cm²). Mihailtchi *et al.* [23] presented 17.4 % efficient *n*⁺*np*⁺ solar cells (140 cm²) made on 31 Ωcm FZ Si wafers.

1.4 This work

In this work, we focus on back junction n^+np^+ solar cells featuring a full-area screen-printed aluminium-alloyed rear p^+ emitter. In order to exploit the advantages of the excellent electrical properties of the n -type Si bulk material, an adequate passivation of the Al-doped emitter is essential. Therefore, we investigate two different passivation layers:

(i) Amorphous silicon layers formed by means of plasma-enhanced chemical vapour deposition (PECVD): Recently, excellent passivation properties of a-Si films have been proven on boron-diffused and aluminium-alloyed emitters. Emitter saturation current densities J_{0e} of lower than 100 fA/cm² have been achieved on 30–225 Ω/sq boron-doped p^+ emitters with a minimum J_{0e} value of 24 fA/cm² for a sheet resistance of 225 Ω/sq by applying amorphous silicon/silicon nitride double layers [24, 25]. On etched 70 Ω/sq Al-doped p^+ emitters, J_{0e} values of 250 fA/cm² have been obtained using single a-Si layers, corresponding to implied open-circuit voltages $V_{oc,impl}$ above 660 mV [26].

(ii) Aluminium oxide layers prepared by plasma-assisted atomic layer deposition (ALD):

Al₂O₃ has been demonstrated to create a high-quality field effect passivation as it contains a high fixed negative charge density up to 10¹³ cm⁻² which effectively shields electrons from the Si surface [27]. The Al₂O₃ films limit the emitter saturation current density of B-diffused p^+ emitters to 10 and 30 fA/cm² on > 100 and 54 Ω/sq emitters [28]. Applying ALD Al₂O₃ layers to boron-doped p^+ emitters, Benick *et al.* achieved an efficiency of 23.2% for a front junction n -type PERL solar cell with an open-circuit voltage of 704 mV [4].

As for our n^+np^+ solar cells the Al- p^+ emitter is located at the cell's rear, we cover both passivation layers by PECVD silicon oxide to increase the internal reflectance. Additionally, the thermal stability of a-Si films is improved by a covering SiO_x layer [29].

The two main challenges of this work are: (i) implementation of an effective passivation for Al-doped emitters into our n^+np^+ cell process and (ii) demonstration of the high potential of Al- p^+ emitters for n -type Si solar cells. We first of all describe in detail our n^+np^+ solar cell structure and the processing sequence. Subsequently, we present results and characteristics for our n -type cells featuring full-area screen-printed aluminium-alloyed rear p^+ emitters passivated by a-Si/SiO_x and Al₂O₃/SiO_x stacks, respectively.

2 SOLAR CELL FABRICATION

2.1 Cell Structure

We fabricated n^+np^+ solar cells with a high-efficiency front side consisting of (i) a textured surface with inverted pyramids, (ii) a phosphorus-diffused n^+ region with a sheet resistance of 120 Ω/sq, acting as a front-surface field (FSF) and providing a good electrical contact to the base, (iii) a thermally grown silicon oxide layer as surface passivation and antireflection coating and (iv) a contact grid formed by evaporation of a TiPdAg seed-layer followed by silver plating. On the rear, we investigate and compare three different kinds of passivation for full-area Al- p^+ emitters: (i) without

additional passivation layer, emitter entirely contacted, (ii) with a-Si/SiO_x passivation stack, contacted via point contacts and (iii) with Al₂O₃/SiO_x passivation stack, contacted via point contacts. Figure 1 shows the schematic cross sections of the realised n^+np^+ rear junction cell structures with non-passivated and passivated aluminium emitters, respectively.

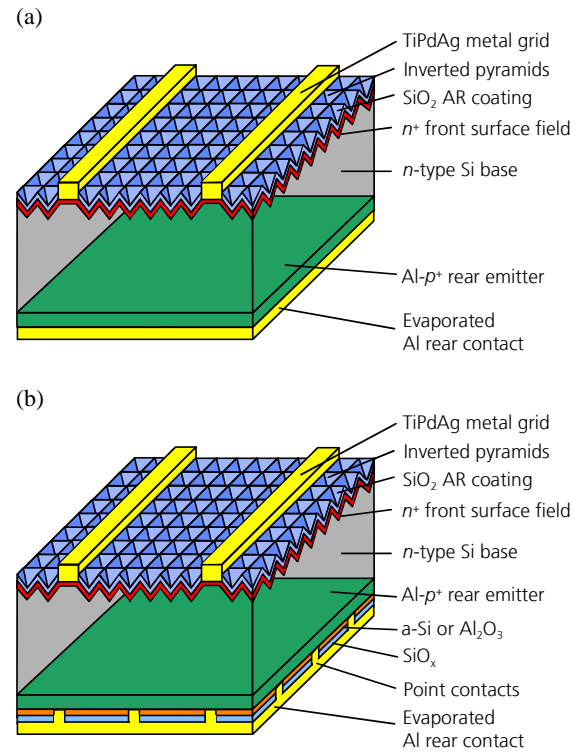


Figure 1: Schematic cross sections of n^+np^+ n -type Si solar cells with full-area screen-printed aluminium-alloyed rear p^+ emitter:

- (a) non-passivated Al- p^+ emitter,
 (b) a-Si/SiO_x- and Al₂O₃/SiO_x-passivated Al- p^+ emitter, respectively.

2.2 Processing Sequence

In this study, we used n -type phosphorus-doped float-zone silicon wafers with a resistivity of 10 Ωcm as base material for our n^+np^+ solar cells. For this material we have measured extremely high effective lifetime values τ_{eff} up to 10 ms using quasi-steady-state photoconductance (QSSPC) and photoluminescence (QSSPL) methods, see Figure 2 [30]. Both surfaces of these lifetime samples are passivated by a 120 Ω/sq n^+ diffusion and 105 nm thick thermally grown SiO₂ layers.

After removal of the saw damage from the starting wafer, a silicon oxide etching mask for inverted pyramids is grown by a dry thermal oxidation in an open quartz-tube furnace. After photolithographically structuring the oxide on the front surface and texturing the wafer in KOH solution, this oxide layer acts as diffusion barrier on the rear side during the subsequent POCl₃ diffusion to form a phosphorus-doped n^+ front-surface field with a sheet resistance of about 120 Ω/sq. In the next step, a short dip in HF solution removes the phosphorus glass on the front and the oxide mask on the rear. After that, a 105 nm thick antireflection oxide layer is thermally grown and removed from the rear. Now, a non-fritted

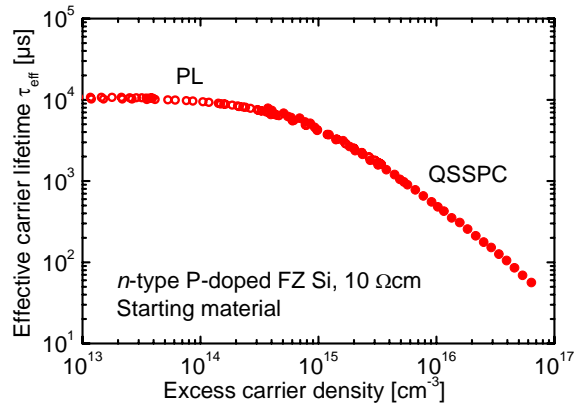


Figure 2: Measured QSSPC and QSSPL lifetime τ_{eff} as a function of the excess carrier density of the n -type phosphorus-doped FZ Si starting material used for cell processing in this work.

aluminium paste is screen-printed onto the entire rear surface and, subsequently, the p^+ emitter is alloyed in a conveyor belt furnace at peak temperatures around 900 °C. After firing, the residue of the aluminium paste and the eutectic layer are etched off in HCl.

At this point of the process, the batch is split up into three parts: (i) cells with non-passivated Al- p^+ emitter, (ii) cells with a-Si/SiO_x-passivated emitter and (iii) cells with Al₂O₃/SiO_x-passivated emitter. To prepare the rear p^+ emitter surface for an effective passivation, we perform a short KOH dip, see section 2.3. After an additional RCA cleaning, for the cells of part (ii) a 70 nm thick PECVD amorphous silicon layer is deposited on the rear Al- p^+ emitter surface at 250°C, and the cells of part (iii) receive a 30 nm thick ALD Al₂O₃ layer at 200 °C at Eindhoven University of Technology, The Netherlands [27]. Then, an additional 150 nm thick PECVD silicon oxide layer is deposited on the rear of the cells of both parts (ii) and (iii) at 260 °C. After that, rear contact points in the SiO_x layer are photolithographically opened followed by plasma etching for part (ii) and an HF dip for (iii) to open the a-Si and Al₂O₃ layer, respectively.

For the following steps, all cells are processed together in one batch again. Now, the full-area aluminium contact is evaporated on the entire rear, and the front contact grid is formed by evaporating Ti, Pd and Ag and a photolithographic lift-off process. After that, the front contacts are thickened by light-induced Ag plating [31] and, finally, the solar cells are annealed in a forming gas ambient at 350–425°C.

2.3 Preparation of Aluminium Emitter Surface

The doping profile of the aluminium-alloyed emitter was detected by electrochemical capacitance voltage (ECV) measurements, see Figure 3. Therefore, we removed the paste matrix consisting of Al-Si particles from the surface and the Al-Si eutectic layer using HCl solution [32]. Subsequently, we cleaned the surface by a short KOH dip to etch off aluminium-rich structures which otherwise would create an Al concentration peak in the doping profile of about 10¹⁹ cm⁻³ close to the surface [26]. A well prepared surface is essential for an effective passivation of the Al- p^+ emitter.

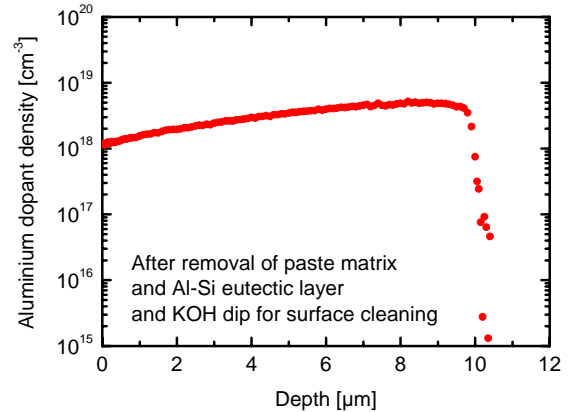


Figure 3: ECV doping profile measurement of the screen-printed aluminium-alloyed rear p^+ emitter of an n^+np^+ Si solar cell.

The thickness of the Al- p^+ region of about 10 μm obtained from the doping profile has also been verified by a scanning electron microscope picture of the cross-section. The interface between the Al-doped p^+ emitter and the n -type Si bulk clearly appears due to the potential contrast, see Figure 4.

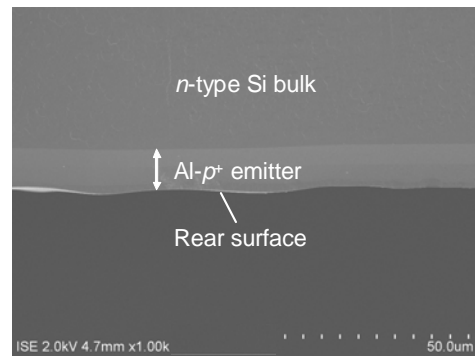


Figure 4: SEM picture of a cross-section of a screen-printed aluminium-alloyed p^+ emitter fired under the same conditions as the sample of Figure 3. The Al-doped p^+ region with a thickness of 10–12 μm is clearly visible.

3 SOLAR CELL CHARACTERISATION

3.1 Solar Cell Results

Table I summarises the electrical parameters of our back junction n -type silicon solar cells featuring differently passivated aluminium-alloyed p^+ rear emitters, fabricated in the course of this work. Figure 5 shows the $I(V)$ curves of these cells measured at Fraunhofer ISE CalLab. The effectiveness of the passivation stacks on the Al- p^+ emitters can clearly be seen from the drastic increase in the open-circuit voltages from 625 mV (non-passivated) to 645 mV (a-Si/SiO_x-passivated) and 649 mV (Al₂O₃/SiO_x-passivated). Our best n^+np^+ solar cell with a-Si/SiO_x-passivated rear p^+ emitter reaches an efficiency of 19.5 %, and our best Al₂O₃/SiO_x-passivated cell achieves an efficiency of 20.1 % which are, to our knowledge, the highest efficiencies obtained so far for n -type Si solar cells featuring aluminium-doped emitters.

Table I: Electrical parameters measured under standard testing conditions (AM1.5G, 100 mW/cm², 25 °C) of n^+np^+ solar cells with full-area screen-printed aluminium-alloyed rear emitter fabricated on n -type phosphorus-doped 10 Ωcm FZ Si wafers. Area (aperture): 2 × 2 cm², thickness: 200 μm. The cells have been processed in the same batch NRE02-T2.

Cell name	Rear Al- p^+ emitter passivation	V_{oc} [mV]	J_{sc} [$\frac{mA}{cm^2}$]	FF [%]	η [%]
1-2	none	625	38.4	79.1	19.0*
2-7	a-Si/SiO _x	645	38.6	78.1	19.5*
3-3	Al ₂ O ₃ /SiO _x	649	39.3	78.9	20.1* **

* Confirmed at Fraunhofer ISE CalLab, Freiburg, Germany

** Al₂O₃ deposited by B. Hoex at Eindhoven University of Technology, The Netherlands

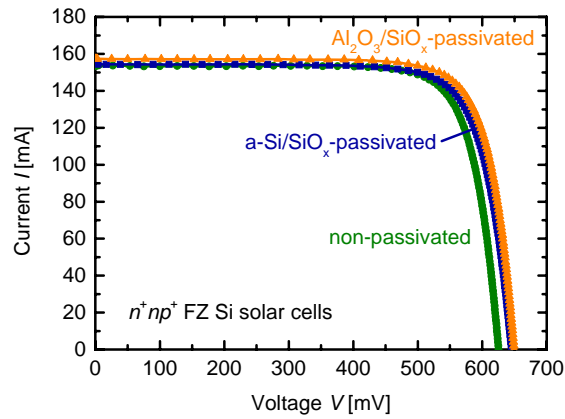


Figure 5: $I(V)$ curves of the n^+np^+ Si solar cells of Table I featuring differently passivated Al- p^+ rear emitters.

To demonstrate the high stability of our cell process, Figure 6 shows the open-circuit voltages V_{oc} and short-circuit current densities J_{sc} of all n^+np^+ Si solar cells processed in this batch. For our a-Si/SiO_x-passivated cells we achieve an increase in V_{oc} of 15–20 mV compared to the non-passivated emitter cells, for our Al₂O₃/SiO_x-

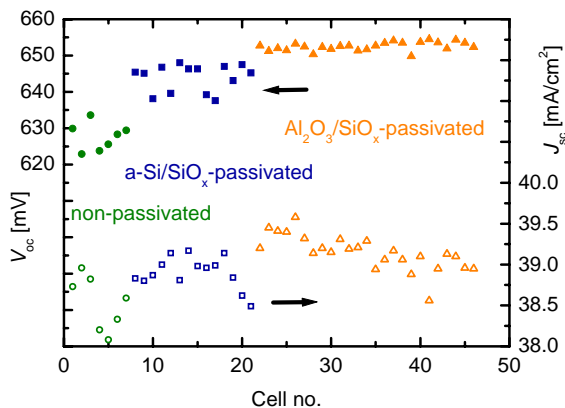


Figure 6: Open-circuit voltages and short-circuit current densities of all n^+np^+ Si solar cells processed in this batch

passivated cells the shift amounts to 25–30 mV, resulting in V_{oc} values up to 655 mV. It is interesting to note that the scattering of the V_{oc} values for the Al₂O₃ cells is smaller than for the cells passivated with a-Si, and this will be investigated in an upcoming publication.

3.2 Solar Cell Quantum Efficiency Analysis

We carried out measurements of the external quantum efficiency EQE and of the hemispherical reflectance R to determine the internal quantum efficiency IQE . EQE and R have been measured with spot sizes smaller than 1 cm² on cell areas without busbars.

Figure 7 shows the $IQE(\lambda)$ curves of the three cells of Table I. High IQE values near 1 are achieved for a wide wavelength range $\lambda = 300\text{--}900$ nm, demonstrating the excellent surface passivation quality of the applied front-surface field including the SiO₂ layer as well as the high minority carrier bulk lifetime of the base material. For long wavelengths above 1000 nm, the IQE curves of the passivated rear emitter cells run significantly higher compared to the IQE of the cell with the non-passivated emitter due to the increased effective diffusion length in the 10 μm thick p^+ emitter and the increased internal reflectance by the a-Si/SiO_x and Al₂O₃/SiO_x stacks, respectively, see Figure 8. The right axis of Figure 7 shows the ratio of the passivated IQE_{pass} and the non-passivated $IQE_{non-pass}$ values to highlight the improvement of the IQE due to the dielectrical passivation layers.

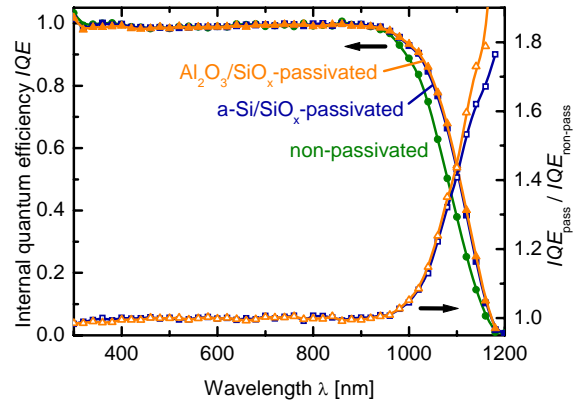


Figure 7: Internal quantum efficiencies of the n^+np^+ Si solar cells of Table I.

Although the internal quantum efficiencies of both passivated emitter cells match very well in the whole wavelength range, the J_{sc} value of the Al₂O₃/SiO_x-passivated cell is significantly higher than the J_{sc} of the a-Si/SiO_x-passivated cell. This difference in J_{sc} results from differences in the reflection as can be seen in Figure 8.

The reflectances in the long wavelength range of both cells with passivated rear emitter are nearly identical which shows that the optical properties of both passivation stacks are very similar and better than those of the non-passivated rear side. The difference in J_{sc} is due to a non-optimal thickness of the front side antireflection oxide layer on the a-Si/SiO_x- as well as on the non-passivated emitter cell as can be seen from the $R(\lambda)$ curves at short wavelengths.

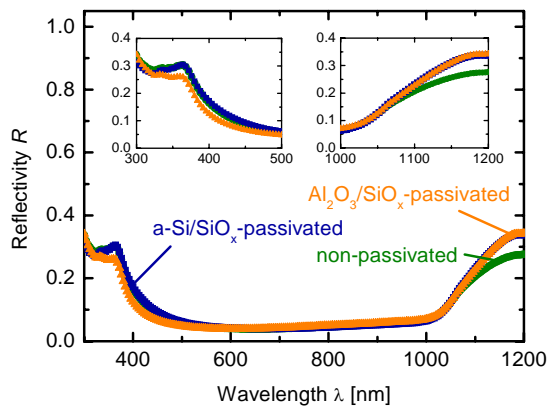


Figure 8: Reflectivities of the cells shown in Figure 7.

3.3 Aluminium Emitter Quality

Our n^+np^+ solar cells show relatively low fill factors of 78–79 %. We determined the pseudo fill factors PFf of the cells of Table I using $SunsV_{oc}$ measurements. PFf values of around 81 % prove the high junction quality of the aluminium-alloyed emitter, see Table II. From this we can conclude that the FF s of our $Al-p^+$ back junction cells are limited by series resistance losses.

Table II: Pseudo fill factors of the cells of Table I measured using the $SunsV_{oc}$ method.

Cell name	Rear $Al-p^+$ emitter passivation	FF [%]	PFf [%]
1-2	none	79.1	81.2
2-7	a-Si/SiO _x	78.1	80.7
3-3	Al ₂ O ₃ /SiO _x	78.9	80.9

4 SUMMARY

We have successfully integrated two different passivation stacks for screen-printed aluminium-alloyed p^+ emitters into our back junction n^+np^+ silicon solar cells. The first one consists of a 70 nm plasma-enhanced-chemical-vapour-deposited amorphous silicon film covered by a 150 nm PECVD silicon oxide layer, the second one of a 30 nm atomic-layer-deposited aluminium oxide also covered by a 150 nm PECVD silicon oxide. Solar cells featuring a full-area screen-printed aluminium-alloyed rear p^+ emitter provided with one of these stacks demonstrate the effectiveness of the passivation by showing an increase in the open-circuit voltage of 15–30 mV compared to cells with non-passivated emitters. This leads to open-circuit voltages around 650 mV. We have proven the high junction quality of $Al-p^+$ emitters by measured pseudo fill factor values of 81 %. For our n^+np^+ solar cells (4 cm²) with a-Si/SiO_x-passivated rear p^+ emitter we have obtained efficiencies up to 19.5 %, and our Al₂O₃/SiO_x-passivated rear emitter cells achieve efficiencies up to 20.1 % on n -type phosphorus-doped 10 Ωcm float-zone silicon material. These are the highest efficiencies reported so far for n -type Si solar cells with aluminium-doped emitters.

ACKNOWLEDGEMENTS

The authors would like to thank B. Hoex, Eindhoven University of Technology, The Netherlands, for the Al₂O₃ depositions. A. Richter is acknowledged for the a-Si depositions. A. Leimenstoll and S. Seitz are gratefully acknowledged for solar cell processing and E. Schäffer for solar cell measurements.

REFERENCES

- [1] D. Macdonald, L. J. Geerligs, Appl. Phys. Lett. **85** (2004), 4061.
- [2] H. Nagel, B. Lenkeit, W. Schmidt, Proc. 22nd EPVSEC, Milan (2007), 1547.
- [3] J. Schmidt, K. Bothe, R. Bock, C. Schmiga, R. Krain, R. Brendel, Proc. 22nd EPVSEC, Milan (2007), 998.
- [4] J. Benick, B. Hoex, M. C. M. van de Sanden, W. M. M. Kessels, O. Schultz, S. W. Glunz, Appl. Phys. Lett. **92** (2008), 253504.
- [5] V. D. Mihailetschi, Y. Komatsu, L. J. Geerligs, Appl. Phys. Lett. **92** (2008), 063510.
- [6] T. Buck, R. Kopecek, J. Libal, R. Petres, K. Peter, I. Röver, K. Wambach, L. J. Geerligs, E. Wefringhaus, P. Fath, Proc. 4th WCPEC, Hawaii (2006), 1060.
- [7] J. Zhao, A. Wang, Proc. 20th EPVSEC, Barcelona (2005), 806.
- [8] J. Zhao, A. Wang, Proc. 4th WCPEC, Hawaii (2006), 996.
- [9] J.-H. Guo, B. S. Tjahjono, J. E. Cotter, Proc. 31st IEEE PVSC, Lake Buena Vista (2005), 983.
- [10] A. Froitzheim, K.A. Münzer, K.-H. Eisenrith, R. Tölle, R.E. Schlosser, M. G. Winstel, Proc. 20th EPVSEC, Barcelona (2005), 594.
- [11] D. De Ceuster, P. Cousins, D. Rose, D. Vicente, P. Tipones, W. Mulligan, Proc. 22nd EPVSEC, Milan (2007), 816.
- [12] S. Taira, Y. Yoshimine, T. Baba, M. Taguchi, H. Kanno, Proc. 22nd EPVSEC, Milan (2007).
- [13] M. Taguchi, H. Sakata, Y. Yoshimine, E. Maruyama, A. Terakawa, M. Tanaka, Proc. 31st IEEE PVSC, Lake Buena Vista (2005), 866.
- [14] E. Conrad, L. Korte, K. v. Maydell, H. Angermann, C. Schubert, R. Stangl, M. Schmidt, Proc. 21st EPVSEC, Dresden (2006), 784.
- [15] A. Cuevas, C. Samundsett, M. J. Kerr, D. H. Macdonald, H. Mäckel, P. P. Altermatt, Proc. 3rd WCPEC, Osaka (2003), 963.
- [16] S. W. Glunz, E. Schneiderlöchner, D. Kray, A. Grohe, M. Hermle, H. Kampwerth, R. Preu, G. Willeke, Proc. 19th EPVSEC, Paris (2004), 408.
- [17] C. Schmiga, H. Nagel, J. Schmidt, Progress in Photovoltaics, **14** (2006), 533.
- [18] P. Hacke, J. Moschner, S. Yamanaka, D. L. Meier, Proc. 19th EPVSEC, Paris (2004), 1292.
- [19] T. Buck, J. Libal, S. Eisert, R. Kopecek, K. Peter, P. Fath, K. Wambach, Proc. 19th EPVSEC, Paris (2004), 1255.
- [20] R. Kopecek, T. Buck, J. Libal, I. Röver, K. Wambach, L. J. Geerligs, P. Sánchez-Friera, J. Alonso, E. Wefringhaus, P. Fath, Proc. 4th WCPEC, Hawaii (2006), 1044.

- [21] C. Schmiga, H. Nagel, R. Bock, J. Schmidt, R. Brendel, Proc. 21st EPVSEC, Dresden (2006), 617.
- [22] H. Nagel, C. Schmiga, B. Lenkeit, G. Wahl, W. Schmidt, Proc. 21st EPVSEC, Dresden (2006), 1228.
- [23] V. D. Mihailetchi, D. S. Sainova, L. J. Geerligs, A. W. Weeber, Proc. 22nd EPVSEC, Milan (2007), 837.
- [24] P. P. Altermatt, H. Plagwitz, R. Bock, J. Schmidt, R. Brendel, M. J. Kerr, A. Cuevas, Proc. 21st EPVSEC, Dresden (2006), 647.
- [25] H. Plagwitz, Y. Takahashi, B. Terheiden, R. Brendel, Proc. 21st EPVSEC, Dresden (2006), 688.
- [26] R. Bock, J. Schmidt, R. Brendel, Appl. Phys. Lett. **91** (2007), 112112.
- [27] B. Hoex, S. B. S. Heil, E. Langereis, M. C. M. van de Sanden, W. M. M. Kessels, Appl. Phys. Lett. **89** (2006), 042112.
- [28] B. Hoex, J. Schmidt, R. Bock, P. P. Altermatt, M. C. M. van de Sanden, W. M. M. Kessels, Appl. Phys. Lett. **91** (2007), 112107.
- [29] M. Hofmann, C. Schmidt, N. Kohn, J. Rentsch, S. W. Glunz, R. Preu, Progress in Photovoltaics, **16** (2008), 509.
- [30] F. Granek, M. Hermle, B. Fleischhauer, A. Grohe, O. Schultz, S. W. Glunz, G. Willeke, Proc. 21st EPVSEC, Dresden (2006), 777.
- [31] A. Mette, C. Schetter, D. Wissen, S. Lust, S. W. Glunz, G. Willeke, Proc. 4th WCPEC, Hawaii (2006), 1056.
- [32] F. Huster, Proc. 20th EPVSEC, Barcelona (2005), 1466.